PRE-BREAKDOWN PHENOMENA IN DIELECTRICS MATERIALS

Kulikov V.
Doctor of Phys.- Math. Sciences. Professor
Tomsk Agricultural Institute, Tomsk, Russia
https://doi.org/10.5281/zenodo.14499282

Abstract

The primary and secondary processes of anodic electrical breakdown in dielectric materials are considered. The primary process of formation of the breakdown channel is caused by the mechanism of generation of free electrons by means of interatomic Auger transitions in the valence band of the dielectric. The secondary processes are connected with destruction of the channel surface by bombardment with accelerated ions in a strong non-uniform field and impact multiplication of ions during collision with conglomerates of atoms of the substance in the region of its gas phase.

Keywords: electrical breakdown of insulators, electrical breakdown mechanisms

Introduction

Electrical breakdown of dielectric materials remains a pressing issue in the development and operation of high-voltage devices and structures. Modern breakdown studies are related to the production of insulators of very complex design using additive manufacturing (3D printing) [1], assessment of the electrical strength of dielectrics of complex composition, in particular various HDPE/PP and LDPE/PP mixtures [2], study of the influence of barriers and interfaces on the electrical strength and service life of insulation samples [3-5], study of the degradation processes of dielectric properties of liquids in a strong electric field [6], and the use of ether liquids as an analogue of mineral oil for transformer equipment [7].

The theoretical model of the electron avalanche by A. von Hippel, H. Fröhlich [8] is used by the authors [for instance, 9-11], but is not dominant at present. Electrical breakdown from the anode (anodic breakdown) in alkali halide crystals (AHC), CdS semiconductor, polymers [12-23], liquid dielectrics [24-26] is satisfactorily described by the mechanism of cascade Auger transitions in the valence band of the dielectric. The appearance, movement and orientation of the electrical breakdown channel are determined taking into account data on the crystal-chemical and energy structure of the substance.

The mechanisms of cathodic breakdown are associated by researchers with the influence of electrons injected from the cathode. In alkali halide crystals, according to the authors of [9], impact ionization and excitation of luminescence centers are observed only in channels of increased electrical conductivity created under the influence of a super-strong electric field. These channels are areas with a modified structure, having a high concentration of linear and point defects.

For polymeric materials, K. Kao [27, 28] proposed a multi-stage process of macromolecule rupture in an electric field. The process includes the injection of electrons from the cathode into the polymer and the capture of the injected electrons with the release of energy approximately equal to the depth of the trap. This energy is transferred to another electron, resulting in the emergence of hot electrons. The latter cause the disintegration of macromolecules into free radicals. The mean free path of electrons increases in areas of lower density (due to the destruction of macromolecules). This creates conditions for impact ionization of molecules, which leads to a sharp increase in current. The released heat initiates the destruction of the polymer and the formation of a breakdown channel.

In dielectric liquids, the discharge glow is associated with the gas phase by the authors of [7, 29]. According to measurements [29], at the first stage there is a continuous spectrum in the region of 480-520 nm, which can be attributed to the dissociation of liquid molecules and the recombination of molecular fragments. At the second stage, almost simultaneously, a line spectrum of the H_a and H_B bands of the Balmer series arises due to the emission of excited hydrogen atoms, and the C_2 Swan series bands of the glow of excited molecules of carbon radicals C_2 [7, 29]. The authors of [30] assume that the injected electrons gain energy in the electric field above the C - H bond energy and cause the dissociation of transformer oil molecules with the formation of hydrogen atoms. The formation of gas bubbles is possible as a result of heating and boiling of the liquid when the injection current flows from the electrode [7, 29-31].

Electrical breakdown in dielectric materials is a complex physical phenomenon, including processes of generation, carrier recombination, charge transfer, and is characterized by high values of temperature, pressure, and carrier concentration in the breakdown channel. In [15, 16, 23], it is shown that the phenomena before breakdown include primary processes of the breakdown channel front movement, conduction current flow, as well as secondary effects associated with increased conductivity and destruction of the channel walls.

In this paper, the modeling of streamers, the main properties of streamers that influence secondary effects, approaches to interpreting the mechanism of increasing conductivity and destruction of capillary walls are presented.

Mechanism of interatomic cascade Auger transitions

Generation of free carriers

Most of the studies of the properties of electrical breakdown have been carried out using alkali halide crystals, as materials with well-studied physical properties. The diagram of the energy bands in the contact

region of a metal electrode and a NaCl sample in a strong electric field is shown in Fig. 1. The crystal is oriented in the <110> direction. The energy levels of the states of the Na and Cl atoms are given in accordance with the data of [33].

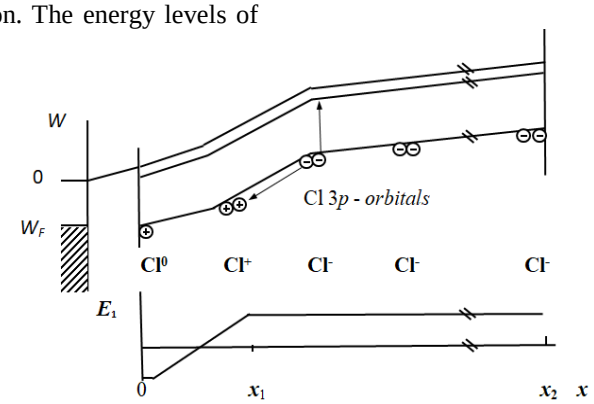

Fig. 1. Scheme of Auger transitions in NaCl *in a strong electric field.* W_c, W_v, W_F *are the energy levels of the conduction band bottom, crystal valence band ceiling and the Fermi metal, respectively;* E_1 *is the electric field of the space charge*

According to [23-25], the onset of the breakdown channel formation is determined by the processes at the metal-dielectric interface. At an average field strength in the sample of ~ 10^6 V/cm, the real strength near the electrode microtips can be more than ~10^8 V/cm. In the near-electrode region of the dielectric, due to the tunnel transition of electrons into the metal, Cl^+ ions with two holes in the 3*p* -orbitals are formed. This requires a voltage *U* such that the edge of the valence band of the dielectric rises to the Fermi level of the metal. In a NaCl crystal, an electron at the 2*p* -level of Na^+ is located ~ 22.4 eV below the bottom of the forbidden band and does not participate in the recombination of the hole on Cl^+. The decay of the hole on Cl^+ occurs as a result of the interatomic Auger transition of an electron from the 3*p* -orbital of the neighboring Cl^- atom and the subsequent generation of an Auger electron in the conduction band (Fig. 1). The Auger transition is possible provided that the minimum energy gap between the 3*p* -levels of chlorine in an electric field is not less than the width of the forbidden band of the dielectric *W*g=8.8 eV. The space charge (SC) includes layers of Cl^0 and a layer of doubly positively charged Cl^+ ions.

A single cycle of the SC front movement in a NaCl crystal can be divided into two successive stages. At the first stage, when the critical local electric field strength of ~ 10^8 V/cm is reached, a hole recombines on Cl^+ due to the interatomic Auger transition of an electron from a neighboring chlorine atom over a time of $\tau_A \sim 10^{-16}$ s and the generation of an Auger electron into the conduction band of the dielectric. The channel moves one interatomic distance (Fig. 1). The negative charge of the electrons lowers the holes charge field and, accordingly, the bending of the bands near the SC boundary. The second stage is associated with the extraction of electrons from the SC region by an external electric field and the achievement of a critical field strength for the implementation of the next cycle. Cycle time Δt can be represented as

$$\Delta t = \tau_A + \tau_1, \qquad (1)$$

where τ_1 - time by electron extraction.

The spatial structure of the breakdown channel is formed by a set of single Auger junction channels (Fig. 1) running in one direction and includes a positive space charge, a heated layer of material, and a conducting channel of complex phase composition with electron-hole plasma. The channel front moves from the positive electrode into the sample.

The concentration of *N* ions in the series of NaCl, KCl, KBr crystals decreases as 5.8, 4.1, 3.4 10^{21} cm^{-3}. According to the mechanism of cascade Auger transitions, the initial concentration of Auger electrons is probably $n_1 \approx N/2 \approx 10^{21}$ cm^{-3}. The recombination process decreases the volume concentration of electrons *n* and holes *p*. The rate of electron recombination can be represented as

$$\frac{\partial n}{\partial t} = -sv_T np - \alpha_B n^2 p \qquad (2)$$

where s ≈ 10^{-13} cm^2 is the cross section of electron capture by a charged center, $v_T \approx 10^7$ cm/s is the thermal velocity of electrons, and a_B is the impact recombination coefficient [16]. The first term on the right-hand side of (2) describes the quadratic recombination of carriers, and the second describes the impact recombination, when, during the recombination of an electron with a hole, part of the energy is transferred to another electron. Impact recombination of charged particles in highly ionized gases predominates over the quadratic one at electron concentrations above ~ 10^{17} cm^{-3} [34]. High values of free electron concentration n in alkali halide crystals can be obtained by irradiation with a high-current electron beam [35]. In single-crystal KCl, KBr, NaCl, the change in

the electron concentration from the beam current density is satisfactorily described by quadratic recombination up to values of $n \approx 10^{16}$ cm^{-3} (excitation current density ~10^3 A/cm^2). Above $n \approx 10^{16}$ cm^{-3}, a sharp decrease in the growth of the electron concentration is observed. The authors of [35] attribute this effect to the capture of electrons by newly generated radiation defects. However, as shown in [36], at high excitation levels (beam current density above 20 A/cm^2), effective depletion of the capture centers by secondary electrons occurs at the stage of their thermalization and, consequently, the effect of concentration saturation can be associated with the onset of impact recombination.

The impact recombination coefficient in KCl and NaCl crystals was estimated in [16] based on the experimental data of [35]. The time resolution of the setup was ~ 0.1 ns, the beam current density was $j = (30-10^4)$ A/cm^2, and the electron pulse duration was ~ 50 ps. At the irradiation stage, the conductivity pulse followed the excitation pulse without inertia, which was observed when the carrier lifetime was shorter than the beam current pulse duration. In this case, the irradiation process could be considered quasi-stationary and the generation and recombination rates could be equated to $G_e = a_B n^3$. The carrier generation rate was calculated using the formula

$$G_e = j\,\Delta W_{0m}/(e\,W_{eh}\,l)\,, \qquad (3)$$

where $j \approx 10^4$ A/cm^2, $\Delta W_{0m} \approx 0.2$ MeV is the average energy of electrons in the beam, $W_{eh} \approx 1.5W_g$ is the average energy of creating an electron-hole pair in the material, e is the electric charge of an electron, $l \approx 150$ μm is the electron range in the sample. According to the results of [16, 35], at the maximum beam current density, the generation rate is ~ 10^{29} cm^{-3}s^{-1}, the electron concentration is in KCl ~ $2\cdot10^{16}$ cm^{-3} and in NaCl ~ $4\cdot10^{16}$ cm^{-3}, the coefficient a_B, neglecting quadratic recombination, is equal to $1.3\cdot10^{-20}$ and $1.6\cdot10^{-21}$ cm^{6}s^{-1}, respectively.

The solution of equation (2) for the concentration n at time t without taking into account the quadratic recombination component has the form

$$n = \frac{n_1}{\sqrt{\alpha_B n_1^2 t + 1}}\,. \qquad (4)$$

Nonradiative recombination of electrons and holes results in heat release and an increase in thermal pressure P_T due to the oscillation of atoms around the equilibrium position. The heat of recombination per unit volume can be estimated as $W_T = (n_1 - n)W_g$. The relationship between thermal pressure and thermal energy per unit volume is given by the equation

$$P_T = \gamma\, W_T, \qquad (5)$$

where γ is the Grüneisen coefficient [37].

An increase in thermal pressure is accompanied by an expansion of the heated volume. The motion of the substance occurs sequentially from the surface boundary to the breakdown channel axis with the speed of sound v_s. In NaCl and KCl samples, the speed of sound $v_s \sim 4.79\cdot10^5$ cm/s and $4.52\cdot10^5$ cm/s, respectively [38]. With a breakdown channel diameter of $d_k \sim 1$ μm, the acoustic relaxation time $\tau_a = (0.5d_k)/v_s \approx 10^{-10}$ s. Acoustic waves arise in a solid provided that the energy input time is less than τ_a.

During time $t \approx \tau_a$, the electron concentration near x_1 drops according to (4) to $n_2 \approx 10^{16}$ cm^{-3}. The energy released per unit volume is $(n_1 - n_2)W_g \approx 1.4$ kJ/cm^3, which is comparable with the heat of fusion for NaCl ~ 1.054 kJ/cm^3 and KCl ~ 0.68 kJ/cm^3, but less than the heat of evaporation 7.98 kJ/cm^3 and 5.5 kJ/cm^3, respectively [38]. The pressure near the boundary x_1, according to (5), is ~ 10^9 Pa. This pressure corresponds to weak shock waves and is capable of deforming the material adjacent to the channel walls.

Probably, the transition heated region is in a solid state, since at such compressions for the transition to the liquid state the heat of fusion is required, which exceeds the heat at atmospheric pressure by 1.5-2 times [37]. This is due to the fact that during the compression of the substance the height of the potential barrier increases, which the ion must overcome in order to leave its crystal lattice site. The length of the transition region of the channel at velocities $v \sim 10^7$ - 10^8 cm/s is $\tau_a \cdot v \sim 10 - 100$ μm. The result of the assessment of the size of the transition region (tens of microns) is in agreement with the data of works [8], where it is shown that the glow in the breakdown channel is associated with a discharge in the gas phase, and the length of the glow and the length of the channel have close values. Considering that the tensile strength of alkali halide crystals does not exceed ~ $5\cdot10^6$ Pa [8], deformations in the heated region along the channel axis, in the direction of the positive electrode, will lead to the destruction of the substance and the formation of a gas phase.

Formation of space charge

The formation of a space charge at the boundary of a conducting layer at $x = x_1$ (Fig. 1) with concentrations of free electrons n and fixed holes p is described by the continuity equations (6) and Poisson equations (7)

$$\frac{\partial \rho}{\partial t} = G - \frac{\partial}{\partial x}\left(en\mu E\right), \qquad (6)$$

$$\frac{\partial E}{\partial x} = \frac{\rho}{\varepsilon\varepsilon_0}\,, \qquad (7)$$

where μ is the electron mobility, ε and ε_0 are the permittivity of the sample and the electric constant, respectively. $\rho = e(p - n)$ is the volume charge density; $E = E_0 + E_1$, is the total electric field strength ($E_0 = U/x_2$ is the external electric field strength, E_1 is the field strength of the space charge Q_s), $G = n_1/\tau_A$ is the volume charge generation rate of Auger electrons in the space from x_1 to $x_1 + \Delta x$; where $\Delta x \sim 4$ Å is the thickness of the atomic layer in the crystal. The Auger generation turn-on time is from t_k to $t_k + \tau_A$, where t_k is the time to reach the critical field strength,

The initial (8) and boundary (9) conditions of the problem will be as follows

$$\text{at } t = 0 \text{ the field strength } E = 0, \qquad (8)$$

$$\text{for } x \geq x_1 \text{ the values } \sigma = 0, \text{ we denote } E_1 = E_s(t), \qquad (9)$$

where $E_s(t)$ is the electric field strength beyond the boundary of the space charge x_1, $\sigma = en\mu$ is the conductivity. The short-circuit condition has the form (10)

$$\int_0^{x_2} E_1 dx = 0\,. \qquad (10)$$

As a first approximation, equation (10) can be represented as

$$E_1 x_1 + E_s\,(x_2 - x_1) = 0\,. \qquad (11)$$

The solution of equations (6) and (7) with the initial and boundary conditions relative to E_1 was obtained in [23] and has the form

$$E_1 = -E_0\left(1 - e^{-\frac{t}{\tau}}\right) + \frac{G\Delta x}{\sigma}\left(1 - e^{-\frac{\tau_A}{\tau}}\right), \qquad (12)$$

where $\tau = \tau_M x_1/(x_2 - x_1)$ is the time constant of the circuit, $\tau_M = \varepsilon\varepsilon_0/\sigma$ is the Maxwell relaxation time. The decrease in the field strength of the positive space

charge E_1 occurs due to the inclusion of the Auger electron field. In the absence of Auger generation, the field strength E in the sample region 0 - x_1 is equal to

$$E = E_0 \, exp\left(-\frac{t}{\tau}\right). \quad (13)$$

In the region x_1 - x_2, the field strength E_s of the space positive charge Q_s, taking into account (12), is determined by the dependence

$$E_s = \frac{E_0 x_1}{(x_2 - x_1)}\left(1 - e^{-\frac{t}{\tau}}\right) \quad (14)$$

In a uniform external field, the strength E_s increases superlinearly with the growth of the coordinate x_1. At $x_1 = 0.5x_2$, the value $E_s = E_0$ with a subsequent sharp increase at $x_1 > 0.7\, x_2$. The spatial structure of the electric field E_1 of the space charge Q_s in the region 0-x_2 is shown in Fig. 1. The value of the positive space charge is determined as

$$\varepsilon\varepsilon_0 E_s = Q_s\left[\frac{k}{cm^2}\right]. \quad (15)$$

The charge Q_s induces a corresponding negative charge in the metal electrodes.

In the case of a non-uniform field, the maximum field strength near the tip E_m in the structure of the "hyperboloid of revolution – plane" electrodes is equal to [39]

$$E_m = \frac{2U}{r\, ln\frac{4d}{r}}, \quad (16)$$

where r is the radius of curvature of the electrode, d is the thickness of the sample. The change in the electric field strength E_x from the coordinate x in the gap 0–x_2 of the dielectric is determined by the expression [39]

$$E_x = \frac{r}{r + x} E_m. \quad (17)$$

The distribution of E_x is non-uniform and obeys the hyperbolic law. In the non-uniform field in the interval 0 – x_2 there is a point x_{mid}, where $E_x(x_{mid})=E_{mid} = U/d$. This means that in the region from the tip electrode to the position x_{mid} the intensity is higher than the average E_{mid}, and in the region from x_{mid} to the flat electrode it is lower. The value $x_{mid} \approx (0.25\text{-}0.3)x_2$. The calculated curves of the distribution of the external field E_x/E_m, in the space 0-x_2 of the sample at r =50 μm are presented in [22].

Pre-breakdown currents

The conduction current density in the space 0 - x_1 is equal to

$$i_1 = \sigma E = \sigma\, E_0 \exp(-t/\tau). \quad (18)$$

The displacement current density in the space x_1 - x_2 has the form

$$i_s = \frac{\partial Q_s}{\partial t} = \sigma E_0\, exp\left(-\frac{t}{\tau}\right). \quad (19)$$

The conduction current densities (18) and displacement (19) are equal.

Currents (18), (19) arise during the formation of the space charge Q_s at the boundary x_1 (σ = 0). At the moment the voltage is turned on, the current $i_1 = \sigma E_0$ and decreases with time according to the exponential law. In the model of the breakdown channel motion at a constant field strength, equation (18) can also be considered as the dependence of the current density on the position of the space charge $Q_s(x_1)$ in the sample at a time different from t = 0. The dependence of the conductivity current density function (18) on the argument $t_1 = x_1/v$ (where v is the breakdown channel velocity, $t_b = x_2/v$ is the breakdown time) for fixed time values $t_{01} = 0.1\tau_M$ (curve 1), $t_{02} = 0.05\ \tau_M$ (curve 2) and $t_{03} = 0.01\ \tau_M$ (curve 3) is shown in Fig. 2. The current density increases slightly with increasing coordinate x_1.

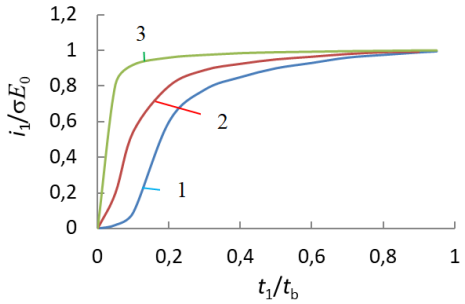

Fig. 2. Dependence of the conduction current density function in the breakdown channel on time

Breakdown channel movement speed

The time τ_1 in formula (1) can be determined from the relationship

$$\tau_1 = Q_A / i_1, \quad (20)$$

where $Q_A = \varepsilon\varepsilon_0 \frac{G\Delta x}{\sigma}\left(1 - e^{-\frac{\tau_A}{\tau}}\right) =$

$G\tau_m \Delta x\left(1 - e^{-\frac{\tau_A}{\tau}}\right)$ - is the charge density of Auger electrons according to expression (12). The product $G\tau_M = (n_1/\tau_A)\tau_M$ characterizes the decrease in the concentration level of Auger electrons under the action of the Maxwell relaxation process. The injection of carriers occurs in a short time and does not depend on the field strength E_0. The cycle time Δt is determined as

$$\Delta t = \tau_A + \frac{G\Delta x \tau_m}{E_0 \sigma} \exp\left(\frac{t_k}{\tau}\right)\left(1 - \exp\left(-\frac{\tau_A}{\tau}\right)\right). \quad (21)$$

Probably $\tau_1 \approx t_k$. The formula for Δt allows us to estimate the dependence of the channel velocity $v(x_1) \approx \Delta x/\Delta t$ on the coordinate x_1. According to (20, 21), the

velocity increases with increasing E_0, conductivity σ and coordinate x_1, due to an increase in current i_1.

Electrical parameters of breakdown

An important characteristic of electrical breakdown is the conduction current. In the experiment, the registration of pre-breakdown currents at the front of the voltage pulse is associated with the need to use bridge measurement circuits to compensate for capacitive recharge currents [40, 41].

Oscillograms of voltage U and pre-breakdown current I in a NaCl crystal with a thickness of ~2 mm with a positive polarity of the tip electrode are shown in Fig. 3 [40].

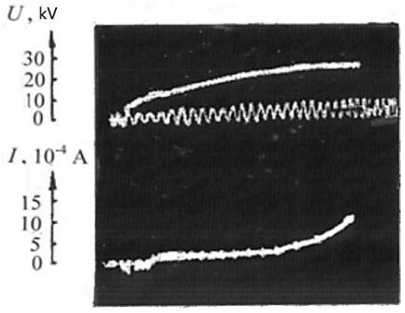

Fig. 3. Oscillograms of voltage pulse U and current I in a NaCl crystal [40]

The beginning of the discharge propagation is noted on the oscillograms by the appearance of a current of the order of ~10^{-4} A (Fig. 3). As the discharge moves deeper into the sample, the current amplitude remains constant and after 1/2 of the breakdown time increases exponentially. The maximum current of ~10^{-3} A corresponds to the time when the breakdown channel reaches the cathode. This is followed by a sharp increase in current, which is not reflected in the photograph. According to the data in [40], the diameter of the breakdown channel is expanded at the anode to ~2-3 μm and narrows towards the cathode to ~0.5 - 1 μm.

As shown above, the amplitude of the pre-discharge current can increase no more than a few percent when passing a channel in the sample. For the primary breakdown, the current density is $i \approx 10^4$ A/cm^2 for a channel diameter of 1 μm. At an average field strength of ~10^5 V/cm, the breakdown front velocity is $v \approx 10^6$ cm/s, and the breakdown time is ≈$2 \cdot 10^{-7}$ s. The conductivity is $\sigma = i/E_{mid} \approx 0.1$ □$^{-1}$ cm^{-1}. The Hall mobility of electrons in the NaCl crystal is $\mu = 20$ cm^2/Vs [42]. Assuming that the mobility in the heated transition layer is $\mu \approx 10$ cm^2/Vs, the electron concentration in the conduction current is $n_2 = \sigma/e\mu \approx 10^{17}$ cm^{-3}, which is close to the theoretical estimate made above.

The dependence of the current on time during breakdown in a water layer 1 cm thick is shown in Fig. 4 [41]. The increase in current near $t \approx 50$ ns corresponds to the beginning of the development of the breakdown channel from the tip. At the initial stages of the increase in the conduction zone into the gap, the current remains constant (~2 A) until the zone dimensions reach ~5 mm, i.e. approximately half the distance from the tip top to the flat electrode. Then the current increases several times before the conductive channel covers the entire interelectrode gap. With an average electric field strength of ~$5 \cdot 10^4$ V/cm, the speed of the breakdown front is ~$6.7 \cdot 10^6$ cm/s.

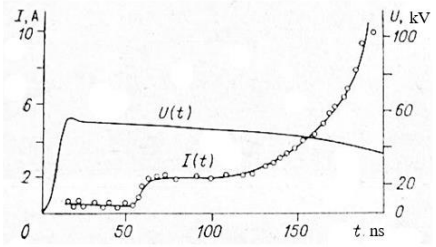

Fig. 4. Pre-breakdown current in water and voltage on the measuring capacitor [41]

The idea of the channel diameter and the speed of its movement in a water gap $d = 800$ μm with a uniform field of ~2 MV/cm according to the data of work [32] is demonstrated by Fig. 5. The time between frames is ~1 ns, the average speed is ~ 10^7 cm/s. The length and diameter of the anode glow increase superlinearly in the process of channel development toward the cathode. The channel diameter near the anode at the initial stage of breakdown (Fig. 5) is $d_k \approx 80$ μm.

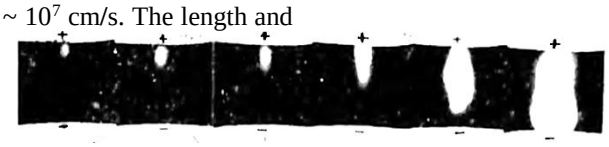

Fig. 5. Change in the length and diameter of the anode glow over time during breakdown in water [32].

With regard to the experiment in Fig. 4, the conductivity current density in water at $d_k \approx 80$ μm is $i \approx 10^4$ A/cm^2, conductivity $\sigma \approx 0.4$ □$^{-1}$ cm^{-1}.

Secondary effects of breakdown

The transverse dimensions of the breakdown channel in AHC are quite stable over its large length [23]. An increase in the channel diameter near the anode surface of the NaCl sample was noted in [40]. The diameter and length of the anode glow in water [32] increase superlinearly in the process of channel development toward the cathode (Fig. 4). In strong electric fields ($E_{mid}>10^6$ V/cm), electrical breakdown in KCl is accompanied by the formation of a hollow ellipsoid in the crystal, located along the channel line [43].

The destruction of the channel surface is probably associated with its bombardment by ions accelerated in a strong non-uniform field in the gas phase of the discharge. In general, ion sputtering begins when the ion energy W_i exceeds the threshold value W_b. The value of W_b weakly depends on the mass of the colliding particles and is in the range of ~10-30 eV. The efficiency of the sputtering process increases with the growth of the mass of the bombarding ions, the angle of incidence of ions from 0 to 40-70^0 and the energy W_i to 70-80 eV [44]. A model of sputtering of two-component materials by light ions is presented in [45]. According to the model, the outgoing flow of atoms is associated with the movement of a certain conglomerate of atoms of both components.

Work on mass spectrometry of plasma clots ejected into a vacuum from the surface overlap region and from breakdown channels in solid dielectrics shows that the main part of the ionic charge is carried by singly ionized molecules. In the case of KCl, there are ions KCl^+, K_2Cl^+, $(K_2Cl_2)^+$, and in the case of polyethylene, there are singly ionized clusters $C_2H_5^+$, $C_4H_9^+$, $C_8H_{17}^+$, consisting of several monomers. The degree of ionization in the breakdown channel in such cases does not exceed 10%. It can be assumed that the main share of neutral particles has the same composition [26, 46, 47].

Most likely, in NaCl and water samples, the impact particles are Na^+ and H^+ ions, and conglomerates of $NaCl^+$ and H_2O^+ are sprayed, respectively. In particular, for positive ions, there is an angular component of the field strength to the surface of the channel wall. The gas phase includes neutral and positively charged ions and conglomerates of atoms of the original substance.

The current increase in the experiment (Fig. 3, 4) can be attributed to secondary breakdown effects. The nature of the current increase corresponds to the exponential law $I(t) \sim 2^n$ (where n is an integer). The start of the current is shifted by time t_g and is probably associated with the beginning of the process of gas phase formation. The drift velocity v_d of a charged particle in the gas phase in a non-uniform electric field E_x is determined as

$$v_d = \mu E_x \qquad (22)$$

The superlinear growth of current $I(t)$ Fig. 3.4 is satisfactorily described by the sum of step functions in the form

$$I(t) = \sum_i I_i \left(t_g + \Delta t_i \right), \qquad (23)$$

where i is the particle number, t_g is the formation time of the gas phase, Δt_i is the delay time of ion motion relative to t_g. For the current I_i, the following notations are introduced: k is the number of steps, □□□is the step duration. Equation (23) is satisfied provided that the Δt_i values of the particles are in a narrow time interval $\Delta t_i <$ □□. The current function of a charged particle I_1 in NaCl and water samples is shown in Fig. 6.

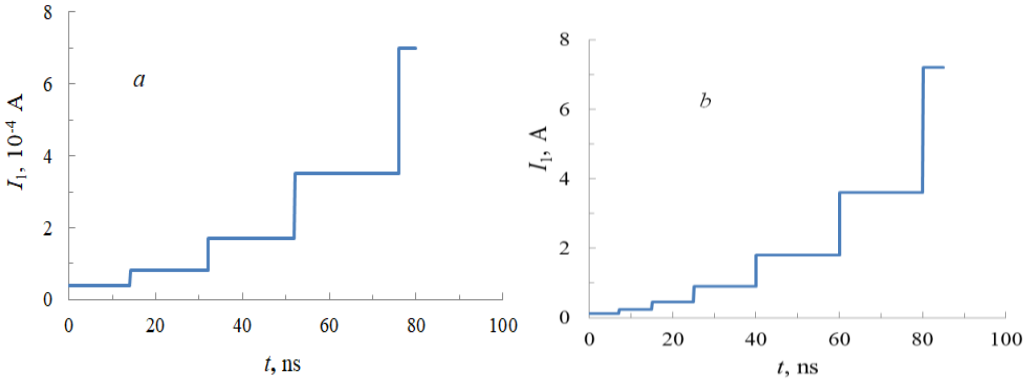

Fig. 6. View of the current function I1 during impact multiplication of charged particles in NaCl (a) and water (b) samples

A characteristic feature of the current structure is its periodic doubling at each time interval □□□which corresponds to the process of impact disintegration of conglomerates of atoms of the substance during bombardment with fast particles. An increase in the duration of the charged particle acceleration period □□ satisfactorily correlates with a decrease in the amplitude of the electric field strength E_x in the tip-plane electrode system. This indicates the movement of an avalanche of positive ions from the anode electrode deep into the sample. Quite large values of □□□, probably include the times of the process of spraying the channel walls with the formation of conglomerates of $NaCl^+$, H_2O^+ and the subsequent reaction of impact multiplication of Na^+ and H^+ ions according to the schemes

$$Na^+ \rightarrow NaCl = Na^+ + NaCl^+, Na^+ \rightarrow NaCl^+ = 2Na^+ + Cl^0, \qquad (24)$$

$$H^+ \rightarrow H_2O = H^+ + H_2O^+, H^+ \rightarrow H_2O^+ = 2H^+ + OH^0. \qquad (25)$$

The rate of reactions (24), (25) is probably limited by the time of formation of conglomerates.

The number of acceleration cycles at half the channel length is $k = 4$ for the sodium chloride sample and k=6 for water, the time of formation of the gas phase is $t_g \approx 80$ ns. The average path between two acts of impact generation z_{mid} in sodium chloride and water is ~250 and ~830 μm. The last acceleration cycles (Fig. 6) are close in time and correspond to motion in the mean field region E_{mid} The drift velocity in this region for sodium chloride is $v_d \approx z_{mid}/\square_\square \approx 10^6$ cm/s and for water $v_d \approx z_{mid}/\square_\square \approx 5.5 \cdot 10^6$ cm/s .

The kinetic energy of Na^+ and H^+ ions in the region of average field strength for sodium ions is 10 eV, for hydrogen ions 15.6 eV. Probably, such energy is sufficient for impact multiplication of ions during fragmentation of conglomerates in the gas phase.

The directed motion of electrons and positive ions under the action of an electric field occurs (due to their "friction" against gas particles) with some constant average velocity v_d. The mobility is inversely proportional to the particle mass. The mobility of ions in the gas phase of the breakdown channel in the region of average field strength, according to (22), is equal to $\mu \approx 10$ cm^2/Vs for Na^+ and significantly greater for H^+ $\mu \approx 110$ cm^2/Vs. According to the data of work [8], under similar experimental conditions, the values of $I(t)$ in the final stage of breakdown are 0.7, 0.3, 0.2 mA for NaCl, KCl, and KBr crystals, respectively. The difference in currents in NaCl and KCl samples probably arises due to the difference in the mobility of Na+ and K+ ions, the masses of which are 23 and 39 a.m.u. The lower mobility of K^+ ions in KBr vapor compared to the mobility in KCl vapor is probably due to the higher scattering cross-section of heavy bromine ions compared to that of chlorine ions in a gaseous medium.

Conclusion

Electrical breakdown in solid and liquid dielectrics can be described by the model of cascade Auger transitions in the valence band of the dielectric. The breakdown channel structure includes a positive space charge, a heated layer of material and a conducting channel of complex phase composition with electron-hole plasma. The gas phase contains neutrally and positively charged ions, conglomerates of atoms of the original substance.

Efficient acceleration of charged particles in the gas phase region, a strong non-uniform electric field contribute to the destruction of the dielectric channel walls. In samples of crystalline NaCl and water, impact bombardment probably occurs with sodium and hydrogen ions in the direction from the anode surface deep into the sample.

Analysis of the pre-breakdown current structure during breakdown in NaCl and water shows that periodic doubling of nonequilibrium carriers corresponds to avalanche generation of ions. The current is caused by the movement of positive Na^+ and H^+ ions.

The kinetic energy of Na^+ and H^+ ions is ~10, 15.6 eV, respectively, which is probably sufficient for sputtering the channel walls and crushing conglomerates in the gas phase.

References:

1. Monzel W. J., Hoff B. W., Maestas S. S., French D. M., Hayden S. C. Dielectric Breakdown of Additively Manufactured Polymeric Materials. IEEE Transactions on Dielectrics and Electrical Insulation. 2015. V. 22. №6. pp. 3543-3549. DOI: 10.1109/TDEI.2015.005199

2. Dabbak S. Z. A., Illias H. A., Ang B. C., Latiff N. A. A. and Makmud M. Z. H. Electrical Properties of Polyethylene/Polypropylene Compounds for High-Voltage Insulation. Energies. 2018. V. 11. P. 1448. DOI:10.3390/en11061448

3. Pattouras M., Tzimas A., Rowland S. M. The effect of material interfaces on electrical tree growth and breakdown time of epoxy resins. IEEE Conf. on Electr. Insul. and Dielectr. Phenom., Shenzhen, China. 2013. pp. 796-799. DOI: 10.1109/CEIDP.2013.6747070

4. Zhang R., Liu X., Zhang T., Xue Ch., Chen H., Li Ya. Electrical Tree Propagation in Composite Insulation for Wind Turbine Generator Under Repetitive Impulse Voltage. Pros. Conf. on Electr. Insul. and Dielectr. Phenom., Toronto, ON, Canada. *2016* .pp. 1007-1010. DOI 978-1-5090-4654-6/16/$31.00

5. Bezprozvannych G.V., Boyko A.N., Roginskiy A.V. Effect of a dielectric barrier on the electric field distribution inhigh-voltage composite insulation of electric machines. Electrical Engineering & Electromechanics. 2018. № 6. pp. 63-67. DOI: 10.20998/2074-272X

6. Bin C., Ji-Wei D., Ming-He C. Electrical Breakdown Mechanism of Transformer Oil with Water Impurity: Molecular Dynamics Simulations and First-Principles Calculations. Crystals. 2021. V. *11*. № 2. P. 123. DOI: 10.3390/cryst11020123

7. Mohan Rao U., Fofana I.,.Beroual A., Rozga P., Pompili M., Calcara L., Rapp K.J. A Review on Pre-breakdown phenomena in Ester Fluids. IEEE Tr. Dielectr. Electr. Insul. 2020. V. 27. № 5. pp. 1546-1560. DOI:10.1109/TDEI.2020.008765

8. Vorobyov A.A., Vorobyov G.A. Electricheskiy proboi i razrushenie tverdykh tel (Izda-vo Vysshaya shkola, M., 1966), 224 s. (in Russian)

9. Vorobyov G. A., Ekhanin S. G. and Nesmelov N. S. Electrical breakdown of solid dielectrics. Phys. Solid State. 2005. V. 47. № 6. pp. 1083-1087. DOI:10.1134/1.1946860

10. Hattori Y., Taniguchi T., Watanabe K. and Nagashio K. Anisotropic Dielectric Breakdown Strength of Single Crystal Hexagonal Boron Nitride. ACS Applied Materials & Interfaces. 2016. 8 (41), 27877-27884

11. Zhao L., Su J. C. and Liu C. L. Review of developments on polymers' breakdown characteristics and mechanisms on a nanosecond time scale. AIP Advances. 2020. V.10. 035206. https://doi.org/10.1063/1.5110273

12. Kulikov V. D. The mechanism of the streamer stage of breakdown in crystal dielectrics. Tech. Phys. Lett. 2000. V. 26. № 2. pp. 170-172. DOI: 10.1134/1.1262781

13. Kulikov V. D. Charge Carrier Generation in a KBr Crystal under the Action of a Pulsed Sub-Breakdown Electric Field. Tech. Phys. Lett. 2002. V. 28. № 2. pp. 99-101.

DOI: 10.1134/1.1458502

14. Kulikov V. D. Electrical Breakdown in Ionic Crystals Exposed to Nanosecond Pulses. Tech. Phys. 2003. V. 48. № 12. pp. 1527-1531. DOI: 10.1134/1.1634672

15. Kulikov V. D. Electrical Breakdown in Ionic Crystals. Tech. Phys. 2009. V. 54. № 1. pp. 56-61. DOI:10.1134/S1063784209010083

16. Kulikov V. D. Model of the Electrical Breakdown Channel in Ionic Crystals. Tech. Phys. 2012. V. 57. № 2. pp. 192-197. DOI:10.1134/S1063784212020144

17. Kulikov V. D. Electrical Breakdown in Ionic Crystals (Izda-vo Tomsk St. Univ. Tomsk, 2014). (in Russian)

18. Punanov I.F., Emlin R. V., Kulikov V. D. and Cholakh S.O. Resistance of a Pulsed Electrical Breakdown Channel in Ionic Crystals. Tech. Phys. 2014. V. 59. № 4. pp. 503-507. DOI: 10.1134/S1063784214040197

19. Emlin R. V., Barakhvostov S. V., Kulikov V. D. Anisotropy of Electrical Breakdown in Crystalline Quartz. Tech. Phys. 2009. V. 54. № 7. pp. 1076-1079. DOI:10.1134/S1063784209070275

20. Kulikov V., Yakovlev V., Bobkova L. Model of a streamer discharge channel in monocrystalline CdS. NJDIS. 2020. № 44-1. pp. 21-24.

21. Kulikov V. Electrical breakdown of polymeric materials. NJDIS. 2021. № 62-1. pp. 51-54. DOI:10.24412/3453-9875-2021-62-1-51-54

22. Kulikov V. Barrier effect in dielectric materials. NJDIS. 2023. № 103. pp. 47-52.

doi. org/10.5281/zenodo.7688048

23. Kulikov V.D. A review on anodic electrical breakdown phenomena in dielectric materials, NJDIS, 2024. №. 128, P. 31. doi: 10.5281/zenodo.10817074

24. Emlin R.V., Punanov I.F., Kulikov V.D. Electronic mechanism of propagation of nanosecond breakdown channel in liquid organic dielectrics. Tech. Phys. 2022. V. 92. № 10. pp. 1342-1348. DOI: 10.21883/TP.2022.10.54361.93-22

25. Kulikov V. Electric Breakdown in Water. NJDIS. 2023. № 118. pp. 50-54.

doi. org/10.5281/zenodo.10009518

26. Emlin R.V., Punanov I.F., Kulikov V.D. Fast breakdown phenomena in liquid dielectrics under pulsed voltage conditions. Proceedings of 9th International Congress on Energy Fluxes and Radiation Effects. 2024 . Tomsk, Russia pp. 917-922. doi: 10.56761/EFRE2024.C2-P-057601

27. Kao K. C. New theory of electrical discharge and breakdown in low-mobility condensed insulators. J. Appl. Phys. 1984. V. 55. № 3. P. 752.

28. Tu N. R. and Kao K.C. High-field electrical conduction in polyimide films. J. App. Phys. 1999. V. 85. P. 7267. doi.org/10.1063/1.370543

29. Sakamoto S., Yamada H.. Optical Study of Conduction and Breakdown in Dielectric Liquids. IEEE Trans. on Electr. Insul. 1980. **EI-15**(3), 171.

30. Yamashita H,, Amano H.. Pre-Breakdown Current and Light Emission in Transformer Oil. IEEE Trans. on Electr. Insul. 1985. **EI-20**(2), 247.

31. Yamashita H,, Ishikawa M., Amano H. Pre-Breakdown density change and current in transformen oil under nouninform field. Proceeding of the 7th International Conference on Conduction and Breakdown in dielectric liquids. 1981. Berlin. pp. 172-176.

32. Ushakov V.Ya. Impul'snyy elektricheskiy proboy zhidkostey. (Izda-vo Tomsk St. Univ. Tomsk, 1975). 258 s. (in Russian).

33. Nemoshkalenko V. V and Aleshin V. G. Electron Spectroscopy of Crystals (Naukova Dumka, Kiev, 1976; Plenum, New York, 1979).

34. Gordiets B. F., Osipov A. I., and Shelepin L. A. Kinetic Processes in Gases and Molecular Lasers (Nauka, Moscow, 1980) (in Russian).

35. Aduev B. P. and Shvaiko V. N., Conductivity of ionic crystals irradiated with picosecond electron beams. Phys. Solid State. 1999. V.41. P.1083.

36. Kulikov V. D. Filling of Traps with Electrons in Insulators Subjected to Intense Electron Irradiation. Tech. Phys. 2007. Vol. 52. No. 5, pp. 559–564.

37. Zel'dovich Ya. B. and Raizer Yu. P. Physics of Shock Waves and High Temperature Hydrodynamic Phenomena (Nauka, Moscow, 1966; Academic, New York, 1967).

38. Shaskolskaya M. I. Acoustic crystals (Nauka, Moscow, 1982). (in Russian).

39. Meek J.M., Craggs J.D. Electrical Breakdown of Gases. (Oxford: Clarendon Press, 1953). 507

40. Torbin N. M. Pre-breakdown currents in large thicknesses of solid dielectrics. Izv. Vuzov. Energetika. 1960. № 10. pp. 26–31 (in Russian).

41. Ovchinnikov I.T., Yanshin E.V. Izmereniye predproboynoy elektroprovodnosti vody s pomoshch'yu impul'snogo vysokovol'tnogo elektroopticheskogo mosta. V kn. Impul'snyy razryad v dielektrikakh. (Izda-vo Nauka, Novosibirsk, 1985), s. 83-88. (in Russian)

42. Seager C.H., Emin D. High-temperature measurements of the electron Hall mobility in the alkali halides. Phis. Rev. B. 1970. Vol. 2, № 8. pp. 3421–3431.

43. Emlin R.V. Punanov I.F. Study of the fine structure of the nanosecond breakdown channel in potassium chloride Phys. Solid State. 2017. V.59. № 8. P. 1565.

DOI: 10.1134/S1063783417080108

44 Behrisch R. Sputtering by Particle Bombardment. (Springger- Verlag, Berlin- Heidelberg- N.Y.- Tokio, 1983)

45. Manukhin V.V. Sputtering of carbide films from the surface of the metal by helium ions bombardment Technical Physics, 2022, Vol. 67, No. 11. P. 1500

46. Emlin R.V., Morozov P.A., Shcherbakov E.N. A mass-charge measurment of main plasma components generated by the dielectric flashover Technical Physics, 2024, Vol. 69, No. 4. pp. 557-563.

47. Emlin R.V., Morozov P.A., Punanov I.F., Lisenkov V.V., Shcherbakov Ye.N. High-Power Plasma Flows Generated by Nanosecond Vacuum Surface Flashover of Polymeric Materials at 80 kV. IEEE Trans. Plasma Sci. 2019. V.47. №. 6. P. 2838, doi: 10.1109/TPS.2019.2914335